International Journal of Applied Earth Observation and Geoinformation 34 (2015) 235–248

Contents lists available at ScienceDirect

International Journal of Applied Earth Observation and Geoinformation

journal homepage: www.elsevier.com/locate/jag

Assessment of RapidEye vegetation indices for estimation of leaf area index and biomass in corn and soybean crops

Angela Kross*, Heather McNairn, David Lapen, Mark Sunohara, Catherine Champagne

Agriculture and Agri-Food Canada, 960 Carling Avenue, Ottawa, Canada K1A 0C6

ARTICLE INFO

Article history:
Received 24 June 2014
Accepted 8 August 2014
Available online 7 September 2014

Keywords:
RapidEye
Leaf area index
Above-ground dry biomass
Vegetation indices
Corn
Soybean

ABSTRACT

Leaf area index (LAI) and biomass are important indicators of crop development and the availability of this information during the growing season can support farmer decision making processes. This study demonstrates the applicability of RapidEye multi-spectral data for estimation of LAI and biomass of two crop types (corn and soybean) with different canopy structure, leaf structure and photosynthetic pathways. The advantages of Rapid Eye in terms of increased temporal resolution (~daily), high spatial resolution (~5 m) and enhanced spectral information (includes red-edge band) are explored as an individual sensor and as part of a multi-sensor constellation. Seven vegetation indices based on combinations of reflectance in green, red, red-edge and near infrared bands were derived from RapidEye imagery between 2011 and 2013. LAI and biomass data were collected during the same period for calibration and validation of the relationships between vegetation indices and LAI and dry above-ground biomass. Most indices showed sensitivity to LAI from emergence to 8 m^2/m^2. The normalized difference vegetation index (NDVI), the red-edge NDVI and the green NDVI were insensitive to crop type and had coefficients of variations (CV) ranging between 19 and 27%; and coefficients of determination ranging between 86 and 88%. The NDVI performed best for the estimation of dry leaf biomass (CV = 27% and r^2 = 090) and was also insensitive to crop type. The red-edge indices did not show any significant improvement in LAI and biomass estimation over traditional multispectral indices. Cumulative vegetation indices showed strong performance for estimation of total dry above-ground biomass, especially for corn (CV ≤ 20%). This study demonstrated that continuous crop LAI monitoring over time and space at the field level can be achieved using a combination of RapidEye, Landsat and SPOT data and sensor-dependant best-fit functions. This approach eliminates/reduces the need for reflectance resampling, VIs inter-calibration and spatial resampling.

Introduction

The availability of information about crop development and health during the growing season can be important for optimizing crop production. Spatially continuous high resolution crop development information can provide producers with relevant information allowing for efficient side-dress fertilizer applications (Scharf and Lory, 2002), irrigation requirements (Bastiaanssen et al., 2000; Hunsaker et al., 2005), disease and weed control (Luedeling et al., 2009; Mahlein et al., 2012), as well as early yield forecasting (Groten, 1993; Mkhabela et al., 2011). Leaf area index (LAI) and biomass are some of the most useful indicators of vegetation development and health for informing these agricultural management practices with respect to adjustments and requirements (Zhang et al., 2002). LAI is also used indirectly as an input variable for primary production models, and crop growth and yield forecasting models (e.g. STICS: Brisson et al., 2003; Steduto et al., 2009; CERES: Fang et al., 2011; Bolton and Friedl, 2013).

LAI and biomass are traditionally estimated through destructive, time-consuming in situ methods; more recent estimates are based on remotely sensed data, such as vegetation indices (VIs). Studies have established relationships between VIs and LAI (e.g. Liu et al., 2012; Nguy-Robertson et al., 2012) and biomass and yield (e.g. Bala and Islam, 2009; Chen et al., 2010; Liu et al., 2010). Overall, VIs show variable sensitivity to different levels of LAI and biomass. The most commonly and widely used index, the normalized difference vegetation index (NDVI) is sensitive to low LAI (i.e. LAI < 2–3), but saturates at medium to high LAI (e.g. Nguy-Robertson et al., 2012). A similar pattern is observed for the relationship between NDVI and biomass, with NDVI saturating at medium to high (fresh) biomass (around 2 kg/m^2, e.g. Chen et al., 2010). A few indices have

* Corresponding author. Tel.: +1 613 415 1507.
E-mail addresses: angela.kross@agr.gc.ca, angelakross@hotmail.com (A. Kross).

http://dx.doi.org/10.1016/j.jag.2014.08.002

shown greater sensitivity to higher LAI and biomass, such as the simple ratio (SR, Nguy-Robertson et al., 2012), the modified triangular vegetation index 2 (MTVI2, Haboudane et al., 2004) and the cumulative MTVI2 (Liu et al., 2009). Indices that incorporate the reflectance of red-edge bands such as the red-edge triangular vegetation index (RTVI) and the modified chlorophyll absorption ratio index (MCARI2) have increased potential for estimating LAI and biomass (e.g. Haboudane et al., 2004; Chen et al., 2010). Most of the reported red-edge indices were derived from narrow band field spectroradiometers (e.g. Viña et al., 2011; Nguy-Robertson et al., 2012), airborne spectrographic imagers (e.g. the compact airborne spectrographic imagery, CASI: Haboudane et al., 2004), or medium resolution spectrometers (e.g. the medium resolution imaging spectrometer, MERIS: Viña et al., 2011). In the application of satellite data to precision agriculture, crop information is required at sufficiently high spatial and temporal resolutions to enable within-field monitoring, the type of data that can be obtained from RapidEye, the first commercial high resolution constellation of satellites with a red-edge band. As a constellation of five, the RapidEye satellites can provide imagery over relatively large areas (swath of 77 km) at a spatial resolution of 5 m and a temporal resolution of 1 day, increasing the successful acquisition of cloud-free data. RapidEye's traditional broadband and red-edge indices were evaluated for grassland nitrogen and biomass (Ramoelo et al., 2012a,b), forest LAI (e.g. Beckschäfer et al., 2014), crop canopy chlorophyll content (Vuolo et al., 2010) and wheat ground cover and LAI (Jiali et al., 2012). Yet, its utility for LAI and biomass estimation in corn and soybean is not well documented. This study addresses this research gap by evaluating the applicability of RapidEye data for soybean and corn LAI and biomass monitoring. A multi-sensor approach using RapidEye data in combination with Landsat and SPOT data was also investigated for continuous field-level crop LAI monitoring. VIs based on combinations of reflectance in green, red, red-edge and near infrared bands were explored. Considering the saturation of VIs, the study also explored indices that have shown low or no saturation to high LAI or biomass such as the SR, MTVI2 and RTVI (Nguy-Robertson et al., 2012; Haboudane et al., 2004; Chen et al., 2010, respectively).

The study was conducted in eastern Ontario, Canada. Corn and soybean are the two most abundant crops in this region. In 2013 these two crops had a combined harvested area of ~70% (~18.20×10^3 ha) of the total field crop area of Ontario (hay area not included, OMAFRA, 2014). The specific objectives of this study were to: (1) to explore relationships between RapidEye derived vegetation indices and LAI and biomass; (2) to determine transfer functions for estimation of LAI and biomass of two crop types (corn and soybean) with contrasting leaf structures (monocot vs. dicot), canopy architectures (erectophile vs. planophile leaf angle distribution) and photosynthetic pathways (C4 vs. C3), without individual crop parameterization; and to develop LAI and biomass maps with associated measures of uncertainty and (3) to investigate Landsat and SPOT derived LAI for continuous multi-sensor field-level crop LAI monitoring.

Methods

Study area and cropping systems

The study site was located within an experimental watershed area (~950 ha) in eastern Ontario, Canada (45.26 N, 75.18 W). The area is characterized by dominant silt loam soils, low topographic variations (slopes < 1%) and humid continental climate (Cicek et al., 2010). Agriculture is characterized by one harvest per year, with corn and soybean being the dominant crops. More details about this area are described in Cicek et al. (2010) and Crabbé et al. (2012).

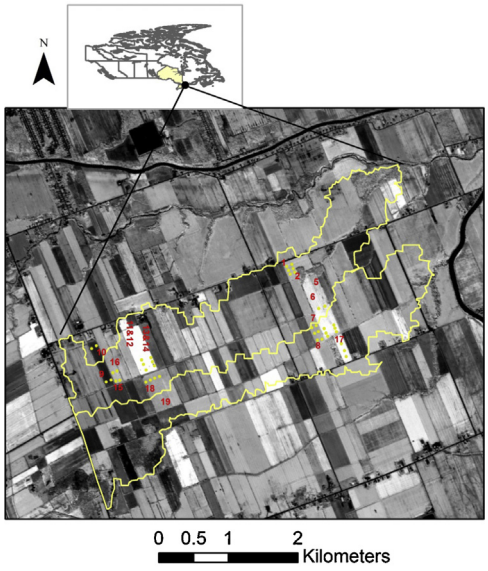

Fig. 1. Overview of the location of the study area (yellow polygon) within Ontario, Canada (inset) and the sampling fields (numbers) and sites (yellow dots).

The study was conducted during the crop growing seasons (May to October) for the years 2011, 2012, and 2013. The regional 30-year normal annual precipitation is 963 mm and average minimum and maximum air temperatures are 0.9 and 11.4 °C, respectively (EC, 2014). Average 30-year precipitation and mean 30-year minimum and maximum air temperatures during the growing season (May–October) are 506 mm, 10.3, and 21.0 °C, respectively (EC, 2014). Total growing season rainfall was 462 mm, 410 mm, and 598 mm for 2011, 2012, and 2013, respectively. Average growing season temperature was 16.5 °C, 16.6 °C, and 15.6 °C for 2011, 2012, and 2013, respectively.

Corn (*Zea mays* L.) and soybean (*Glycine max* L.) crops were grown on the experimental fields where in situ data was collected (Fig. 1). Agronomic practices are conventional for row crop agriculture in this region of Canada (OMAFRA, 2013). Tillage practices typically consist of fall moldboard plowing and spring cultivation using chisel style implements. Generally, crops are planted in early to late May and harvested between late September and early November. Crop row spacing is generally 40–50 cm for soybean and 60 cm for corn. Soybean crops in fields 1 and 2 for 2011 and 2012 were planted with a twin-row cropping system. Soybean and corn plant densities were generally 354,000 and 64,200 plants/ha, respectively (Sunohara et al., 2014a). Fertilizer generally consists of broadcast application of granular urea prior to planting and a granular starter application. Fertilizer rates are generally ~170 kg N/ha for corn, ~3 kg N/ha for soybean, depending on soil and crop requirements. Fields 18 and 19 received liquid dairy manure applications (at rates ~70,000 L/ha) in the fall of 2011 and spring of 2012 (Sunohara et al., 2014b). A fall application of municipal bio-solids was applied in 2012 to fields 7 and 8.

In situ data

Two to three sampling sites were selected per field from 15 agriculture fields in the study area (Fig. 1). Measurements were conducted at weekly intervals during the crop growing season (May–October); at each LAI sampling site 14 digital hemispherical photos (Nikon DS300 camera with a F12.5 mm fisheye lens) were collected every 5 m along two parallel transects separated by 5 m. The use of transects for indirect LAI estimation over crop rows has been previously supported and tested successfully (e.g. Strachan

et al., 2005; Canisius et al., 2010). LAI was estimated from the digital hemispherical photos using the Can-Eye software, version 6.2 (*http://www6.paca.inra.fr/can-eye*).

Above-ground crop biomass was collected from the LAI sampling sites in 2012 and 2013. At each sampling site 10 plants were collected (from two randomly selected adjacent rows within the sampling site); the plants were separated into leaves, stems and fruits/seeds and were dried in an oven for about 72 h at 80 °C. The dry biomass was weighted and scaled to leaf and total biomass per m^2 using plant density (which was measured as the average number of plants along 10 m within a row and across 10 rows).

Satellite data

A total of 32 RapidEye images were used from the growing seasons of 2011–2013 (Table 1). All images were orthorectified in PCI's OrthoEngine (PCI Geomatica v10.3), using the image's rational functions. Additional GCPs were manually collected using an Ontario road map that was derived from the National Topographic Data Base, Canada (NTDB, 2007). The images were then atmospherically corrected using PCI's ATCOR2 (PCI Geomatica v10.3). Cloud masks were manually created for all images and all image values under the cloud masks were set to NoData. To evaluate the use of Landsat and SPOT data for field-level multi-sensor LAI monitoring, two Landsat and three SPOT images were obtained for 2011 (Table 1). SPOT images were ortho-rectified in PCI's OrthoEngine; and both SPOT and Landsat images were atmospherically corrected using PCI's ATCOR2.

Vegetation indices

Indices selected for evaluation used a combination of visible, near-infrared and red-edge bands (Table 2), including: NDVI, SR, red edge normalized difference vegetation index (NDVIre), red edge simple ratio (SRre), green NDVI (gNDVI), MTVI2, core red edge triangular vegetation index ($RTVI_{core}$). The NDVI, SR, gNDVI, MTVI2, the land surface water index (LSWI) and moisture stress index (MSI) were computed from the SPOT and Landsat images.

From all images, zonal statistics of the ground LAI sampling sites were extracted using a rectangular buffered area of about 50 m × 50 m. Only images within ±3 days of the ground data collection dates were included in the analysis. For estimation of LAI from RapidEye there were 139 matching LAI site-observations (Table 1) and 30 matching biomass site-observations (12 corn, 18 soybean). For Landsat and SPOT there were respectively 10 and 13 matching LAI site-observations (Table 1).

The applicability of both VIs and cumulative VIs was evaluated for estimation of total biomass. Cumulative VIs have been used as a proxy for absorbed photosynthetically active radiation (APAR, e.g.: Liu et al., 2009) which is proportional to total biomass (Monteith, 1972). For each biomass sampling site, daily VI time-series were created from all the multi-temporal RapidEye images (Table 3) using a logistic function (Zhang et al., 2003, Fig. 2). Cumulative VIs (i.e. igNDVI, iMTVI2, iNDVI, iNDVIre, iSR, iSRre, $iRTVI_{core}$) were calculated using numerical integration in Matlab v. R2013. There were 48 biomass sampling site-observations (24 corn, 24 soybean); each sampling site observation was matched with the cumulative VI value from day of year (DOY) 140 (representing the approximate baseline for VIs, corresponding to approximate planting date) to the date of the biomass sampling.

Analysis

Matlab's (v. R2013) curve-fitting toolbox was used to evaluate the best-fit linear and non-linear relationships between VIs and LAI and biomass (i.e. objective #1). The relationships were assessed through goodness-of-fit measures obtained from the curve-fitting analysis, including the coefficient of determination (r^2) and the root mean squared error (RMSE).

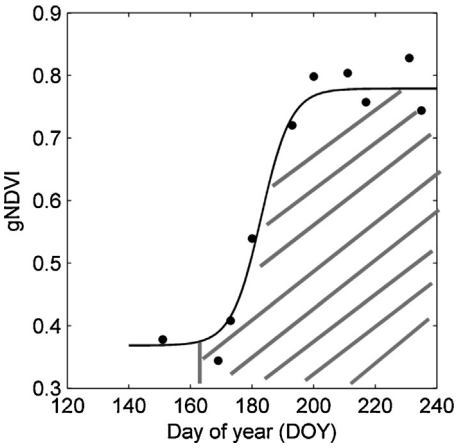

Fig. 2. Example of the curve-fitting approach used for calculation of the area under the curve. Black dots are gNDVI values from RapidEye imagery of different dates within 2012. gNDVI is fitted against the time using a logistic function. The striped area under the fitted curve is calculated through numerical integration.

An independent validation was performed to determine the final best-fit models (i.e. objective #2). In this analysis 70% of the sampling site-observations were used for calibration and 30% for validation. In addition to r^2 and RMSE, the mean absolute error (MAE) and the coefficient of variation (CV) were also reported to evaluate the fit of the models. RMSE and MAE characterize the mean differences between measured and estimated variables: MAE is less sensitive to extreme data values (Willmott, 1982). CV gives an indication of the difference compared to the mean of the observed variable (calculated as the ratio of RMSE and the mean of the measured variable multiplied by 100).

In practice, the usefulness and the operational value of VIs for estimation of plant biophysical variables increases when there is no need for model parameterization for each crop type. In this study, r^2 values of the relationships between most of the VIs with LAI and leaf biomass were high (>80%) for the two crops combined (and for the individual crops). To test the robustness of the pooled regression models (based on the two crops combined), errors of estimated LAI and leaf biomass of each individual crop were compared with errors of estimated LAI and leaf biomass when the two crops were combined. In addition, an *F*-test statistic was calculated to verify if the regression coefficients of the pooled data and the regression coefficients of the individual crop data were equal (Chow test, Chow, 1960). When *p*-values were larger than 0.05, the VI was determined as being insensitive to crop type, meaning that the pooled regression model can be used for estimating LAI or leaf biomass in both corn and soybean fields.

For total biomass, r^2 values of the relationships between integrated VIs and total biomass were lower for the two crops combined (54–75%), than for the individual crops (up to 92%); therefore individual crop specific regression models were used to estimate the total biomass of corn and soybean.

To investigate Landsat and SPOT derived LAI for continuous multi-sensor field-level LAI crop monitoring (i.e. Objective #3), LAI estimated from matching dates was compared for RapidEye and Landsat (image from 5 July 2011) and RapidEye and SPOT (image from 22 July 2011). The comparison was made between field averages. A total of 109 fields (66 corn fields, 43 soybean fields) were used for the RapidEye-Landsat comparison, and 110 fields (66 corn fields, 44 soybean fields) were used for the RapidEye-SPOT

Table 1
Overview of imagery dates and number of matching LAI site-observations.

Year	Matching[a] RapidEye	Matching[a] Landsat	Matching[a] SPOT
2011	27-June-2011 05-July-11 12-August-11 19-August-11 26-August-11	19-June-11 05-July-11	16-June-11 28-July-11 23-August-11
2012	17-June-12 21-June-12 28-June-12 11-July-12 18-July-12 29-July-12 04-August-12 22-August-12		
2013	12-June-13 19-June-13 26-July-13		
Corn sampling site-observations	55	6	11
Soybean sampling site-observation	84	4	2
Total sampling site-observations	139	10	13

[a] "Matching" refers to the images that matched ground data collection dates.

Table 2
References and equations of VIs used in this study.

Index	Acronym	Equation	Reference
Green NDVI	gNDVI	$(R_{NIR} - R_{green})/(R_{NIR} + R_{green})$	Gitelson et al. (1996)
Normalized difference vegetation index	NDVI	$(R_{NIR} - R_{RED})/(R_{NIR} + R_{RED})$	Rouse et al. (1974)
Simple ratio	SR	R_{NIR}/R_{RED}	Jordan (1969)
Red edge normalized difference vegetation index	NDVIre	$(R_{NIR} - R_{RED\text{-}edge})/(R_{NIR} + R_{RED\text{-}edge})$	Gitelson and Merzlyak (1994)
Red edge simple ratio	SRre	$R_{NIR}/R_{RED\text{-}edge}$	Gitelson and Merzlyak (1994)
Modified triangular vegetation index	MTVI2	$1.5[1.2(R_{NIR} - R_{GREEN}) - 2.5(R_{RED} - R_{GREEN})]/\sqrt{[(2R_{NIR} + 1)^2 - (6R_{NIR} - 5\sqrt{(R_{RED})}) - 0.5]}$	Haboudane et al. (2004)
Red edge triangular vegetation index (core only)	$RTVI_{core}$	$100(R_{NIR} - R_{RED\text{-}edge}) - 10(R_{NIR} - R_{GREEN})$	Chen et al. (2010)
Normalized difference water index or Land surface water index	NDWI, LSWI	$(R_{NIR} - R_{SWIR})/(R_{NIR} + R_{SWIR})$	Gao (1996)
Moisture stress index	MSI	R_{SWIR}/R_{NIR}	Rock and Vogelmann (1985)

Table 3
Overview of RapidEye imagery used for the calculation of cumulative indices.

Year	Month	Image – day of month	Biomass site-observations
2012	May June July August	30 17, 21, 28 11, 18, 29 4, 18, 22, 29	30 biomass site observations (12 corn, 18 soybean)
2013	May June July August	18, 27, 30 12, 19 6, 15, 20, 26 5, 10, 17,21, 29	18 biomass site-observation (12 corn, 6 soybean)

comparison. The comparison was done using boxplots, independent *t*-tests for the mean field LAI, and correlation analysis.

Results and discussion

Relationships between RapidEye vegetation indices and LAI and biomass

In situ measured maximum LAI (between mid-July and mid-August) was lowest in 2011 (on average, 5 m^2/m^2 for corn and 6 m^2/m^2 for soybean) and highest in 2013 (on average 7 m^2/m^2 for both crops). In 2012, maximum average LAI was 6.5 m^2/m^2 for corn and 6 m^2/m^2 for soybean. All VIs were sensitive to the entire range of LAI values (from crop emergence to 8 m^2/m^2, Fig. 3) with varying scatter of data points around the fit line and with r^2 ranging between 0.83 and 0.92 (Fig. 3). Previous studies have shown good relationships between in situ LAI and MTVI2 derived from Landsat data (e.g. Liu et al., 2009), simulated MODIS data (Nguy-Robertson et al., 2012) and hyperspectral CASI data (Haboudane et al., 2004). LAI plotted against RapidEye MTVI2 showed two data clusters for LAI values above and below 3 m^2/m^2 (Fig. 3b). MTVI2 is sensitive to leaf inclination angle (Liu et al., 2012), yet crop type did not explain the pattern in this study as individual crop plots showed similar patterns. The best-fit functions for gNDVI, NDVI and NDVIre $RTVI_{core}$ were linear, but all these indices exhibit some saturation when LAI reaches 6 m^2/m^2 (Fig. 3a, c and d). This sensitivity is still higher than the sensitivity of these indices when derived from other sensors, which have saturated around 4 m^2/m^2 (e.g. Viña et al., 2011; Nguy-Robertson et al., 2012). The $RTVI_{core}$, SR and SRre showed no saturation along the entire LAI range: SR and SRre continue to increase, even after the LAI reaches its maximum value (Fig. 3e–g). Considering that photosynthesis can continue increasing after LAI reaches its maximum, these indices may be indicators of both structural (e.g. LAI) and biochemical properties (e.g. chlorophyll). For SR,

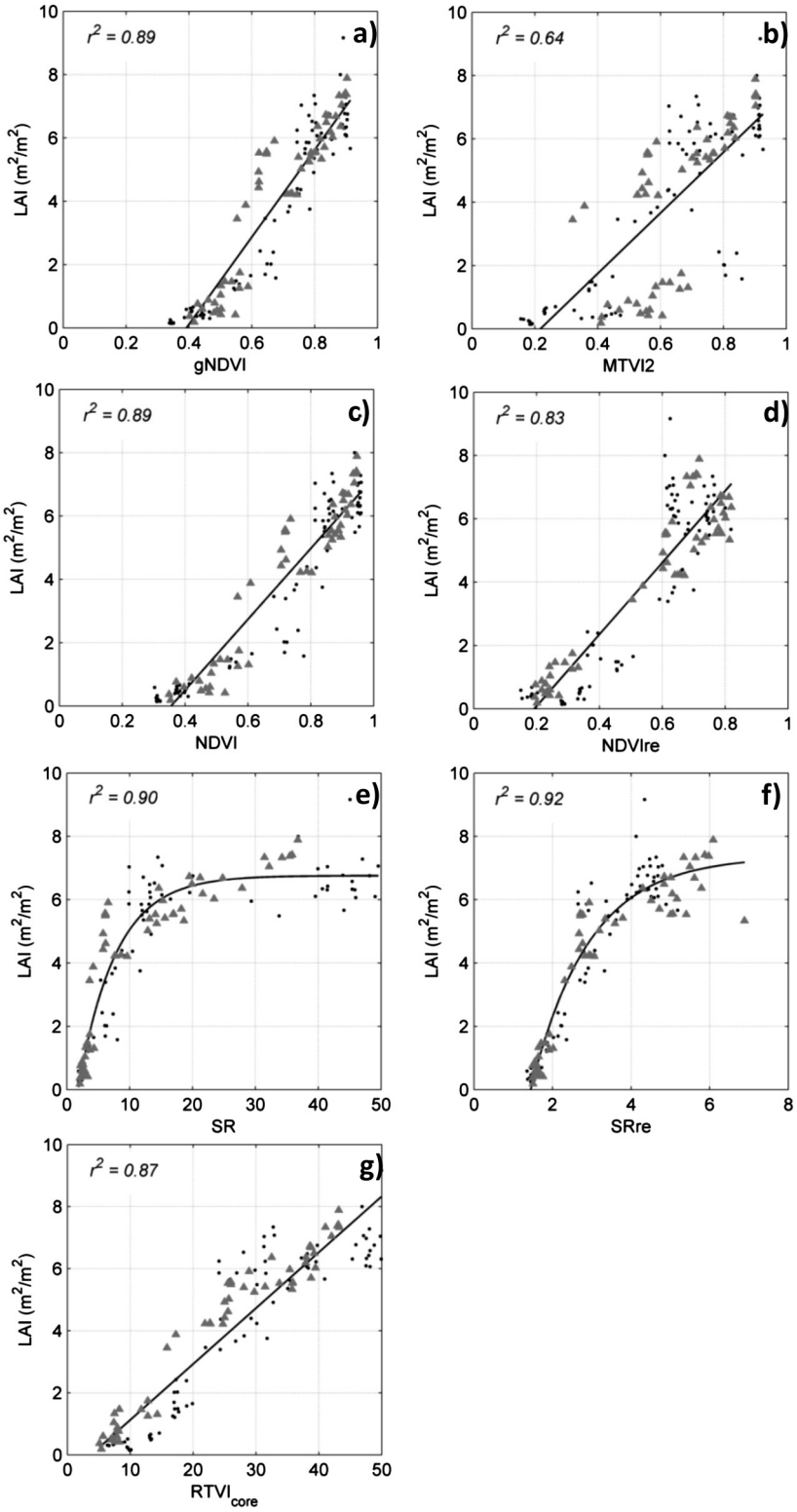

Fig. 3. Leaf area index (LAI, m^2/m^2) plotted against vegetation indices: (a) gNDVI, (b) MTVI2, (c) NDVI, (d) NDVIre, (e) SR, (f) SRre and (g) $RTVI_{core}$. In all panels, dots represent soybean, triangles represent corn. The solid line is the best-fit function for the combined crops. All LAI sampling site observations were used to illustrate the relationships.

this is consistent with Broge and Leblanc (2001) who reported good performance of SR for estimating both LAI and canopy chlorophyll density for vegetation with low density. The results from this study suggest that the SR is also applicable in vegetation with high density, which is consistent with findings from Nguy-Robertson et al. (2012).

Contrary to the LAI relationships, the relationship between MTVI2 and biomass was similar to the relationships between gNDVI and NDVI with leaf and total biomass: all indices became invariant around 400 g/m^2 and around 800 g/m^2 for leaf- and total biomass, respectively (Figs. 4a–c and 5a–c). NDVIre and SRre saturated around the same levels of leaf biomass, followed by a decrease

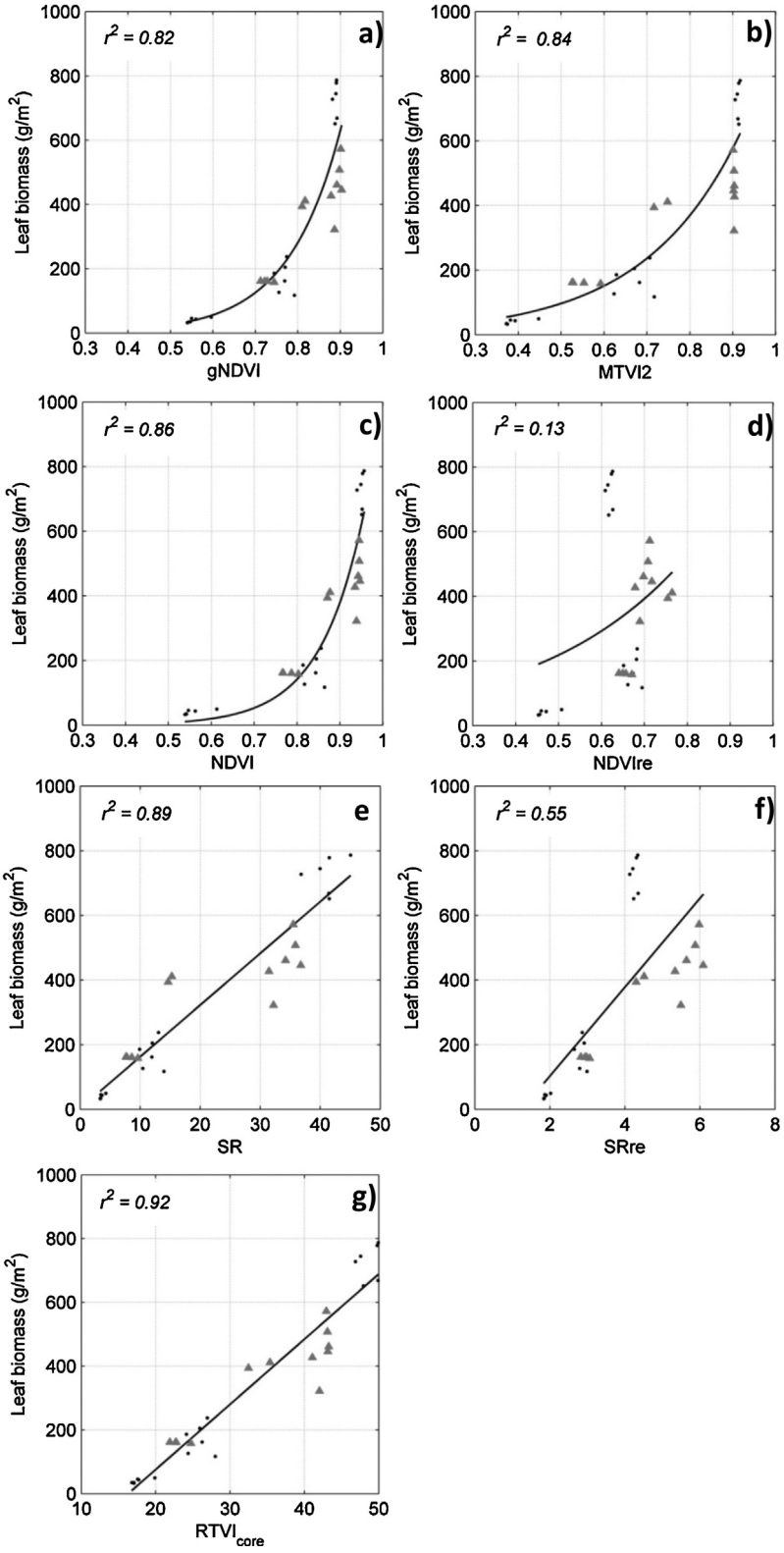

Fig. 4. Leaf dry biomass plotted against vegetation indices: (a) gNDVI, (b) MTVI2, (c) NDVI, (d) NDVIre, (e) SR, (f) SRre and (g) $RTVI_{core}$. In all panels, dots represent soybean, triangles represent corn. The solid line is the best-fit function for the combined crops. All leaf biomass sampling site observations were used to illustrate the relationships.

in the indices (Fig. 4d and f). For total biomass, however, NDVIre had a higher asymptote (Fig. 5d). $RTVI_{core}$ and SR exhibited linear relationships with leaf biomass, with no signs of saturation along the entire range. The relationship with total biomass saturated around 800 g/m^2, followed by a decrease in VI values. Total biomass includes more photosynthetically inactive components (e.g. stem, fruits) than leaf area or leaf biomass, which are likely to affect the relationship between VIs and the photosynthetically active components. Cumulative VIs were a better approach for estimation of total biomass, r^2 values of initial curve fittings (including all data

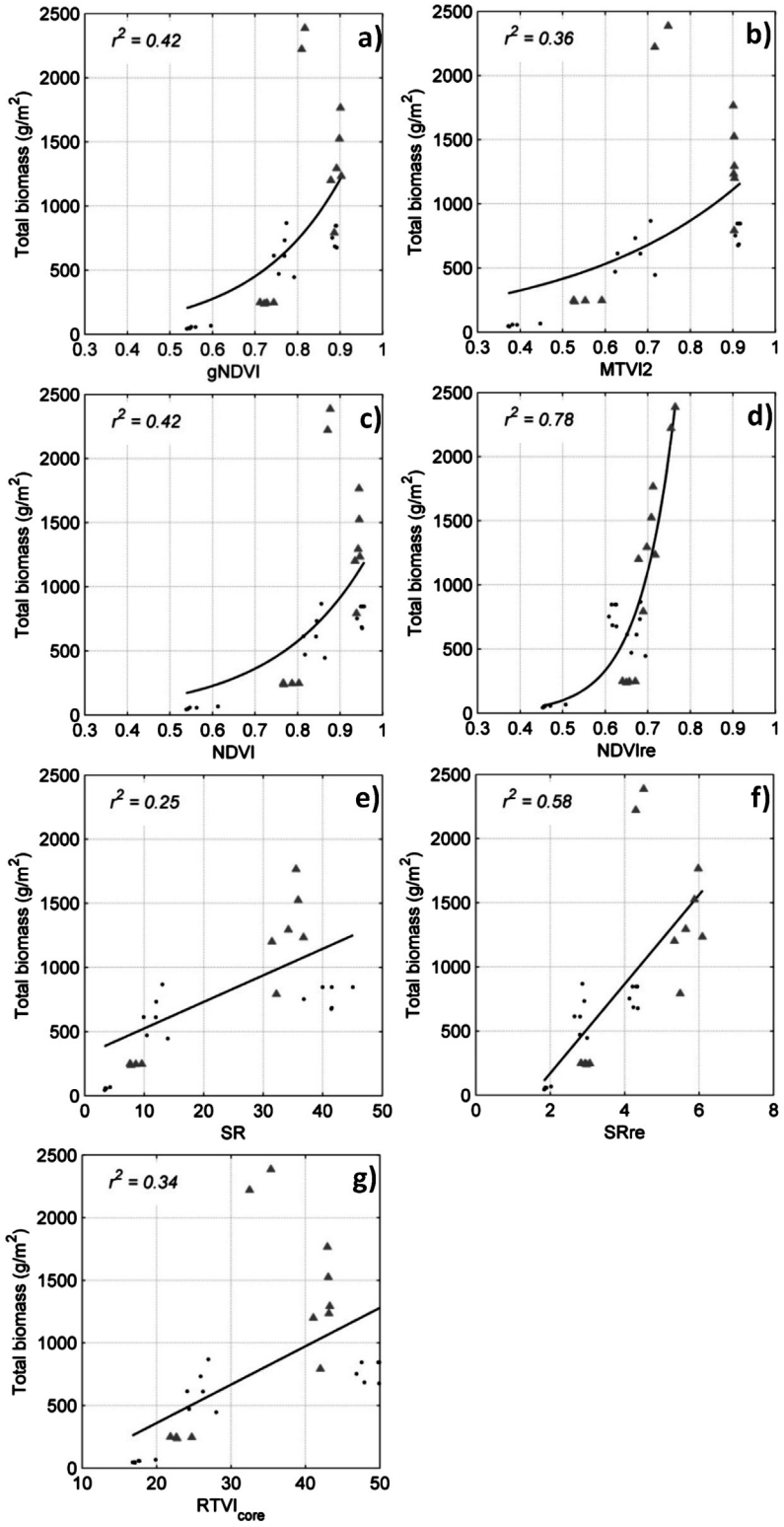

Fig. 5. Total dry biomass plotted against vegetation indices: (a) gNDVI, (b) MTVI2, (c) NDVI, (d) NDVIre, (e) RTVI$_{core}$, (f) SR and (g) SRre. In all panels, dots represent soybean, triangles represent corn. The solid line is the best-fit function for the combined crops. All total biomass sampling site observations were used to illustrate the relationships.

points, $n = 24$ for each crop) ranged between 0.73 and 0.92 for corn (linear relationships for all VIs, Fig. 6); and between 0.66 and 0.93 for soybean (linear and exponential relationships, Fig. 7).

In situ measured LAI reached a maximum while in situ measured biomass continued to increase (Fig. 8). LAI reached its maximum values when leaf and total biomass were around 400 and 800 g/m^2, respectively: the same levels as most of the vegetation indices. This suggests that these indices reflect structural properties (e.g. LAI) and not biochemical properties. Cumulative indices, however, did reflect the biochemical properties.

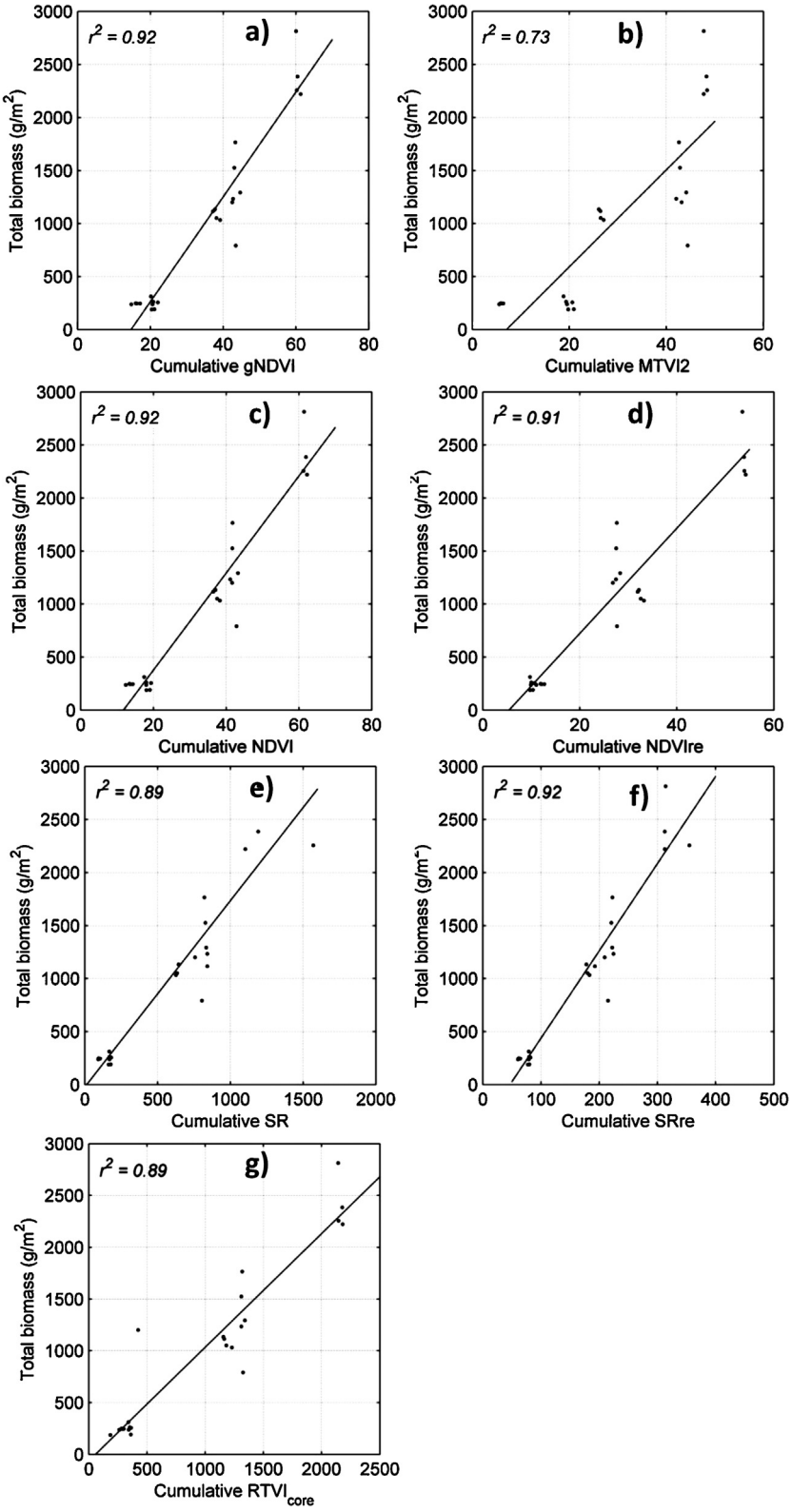

Fig. 6. Relationships between cumulative VIs and total dry corn biomass. All total biomass sampling site observations were used to illustrate the relationships.

Transfer functions for estimation of LAI and biomass

Independent validation of the best-fit functions demonstrated good performance of all VIs (MTVI2 was not selected based on its poor performance in the initial curve fitting analysis) for estimation of LAI of corn and soybean combined (Fig. 3); CV values ranged between 20 and 27%. Two of the red-edge indices ($RTVI_{core}$ and NDVIre) had the highest CV values among all indices, but the NDVIre was insensitive to crop type (Tables 4 and 5), which support findings from Nguy-Robertson et al. (2012). gNDVI, NDVI, SR and SRre had similar errors; CV values were between 18 and 21% for individual and combined crops. Similar error ranges were reported

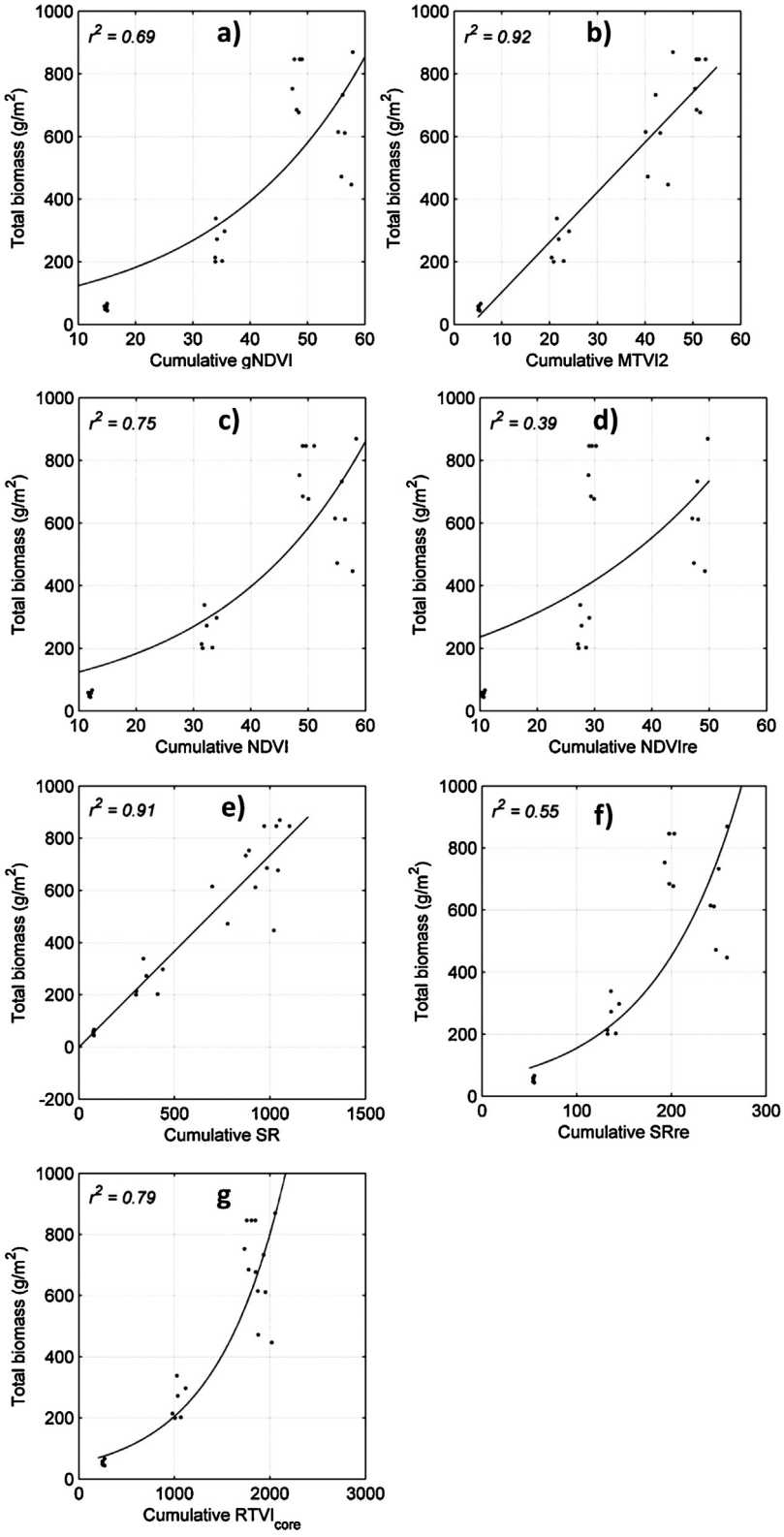

Fig. 7. Relationships between cumulative VIs and total dry soybean biomass. All total biomass sampling site observations were used to illustrate the relationships.

when combining NDVI and SR for estimating low and high LAI, respectively (Nguy-Robertson et al., 2012). The RapidEye indices showed an advantage as they can be used individually for estimation of corn or soybean LAI from emergence to 8 m^2/m^2. gNDVI and NDVI were also insensitive to crop type (Table 4, Table 5). The NDVI was used to create LAI maps for 2012 and 2013, as examples of contrasting exceptional dry (2012) and wet (2013) years (Fig. 9).

For estimation of leaf and total biomass NDVI, $RTVI_{core}$, SR and NDVIre were selected as these indices showed best performance in the initial curve fitting analysis. The independent validation of the relationships resulted in medium to poor performance of all

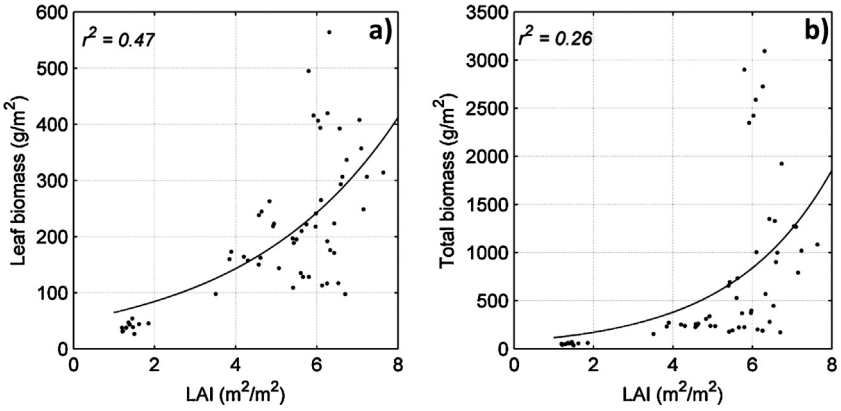

Fig. 8. Scatter plots of in situ measured LAI and (a) leaf biomass and (b) total biomass.

Table 4
Difference statistics of measured and estimated LAI using the pooled regression coefficients (for combined crops).

Transfer function (combined crops)	Errors for corn and soybean combined			
	MAE (m^2/m^2)	CV (%)	r^2	*P*
13.96 * gNDVI – 5.465	0.70	21	0.87	0.2998
11.266 * NDVI – 4.007	0.64	19	0.86	0.0533
11.626 * NDVIre – 2.182	0.85	27	0.88	0.3206
0.181 * RTVI$_{core}$ – 0.639	0.81	24	0.88	0.0036
9.296 * –exp(–0.163* SR) + 6.910	0.50	19	0.94	–
20.17 * –exp(–0.692* SRre) + 7.329	0.49	21	0.93	0.0126

P-value <0.05 indicates that the coefficients of the pooled crop regression model are significantly different from the coefficients of the individual crop regression model (at the 0.05 level). Transfer functions were calibrated on 70% of the 139 sampling site observations and validated on 30% of the sampling site observations. Errors in this table were calculated from the validation dataset.

Table 5
Difference statistics of measured and estimated LAI using the pooled regression coefficients (for individual crops).

Transfer function (combined crops)	MAE (m^2/m^2)	CV (%)	r^2
Errors for corn			
13.96 * gNDVI – 5.465	0.64	22	0.80
11.266 * NDVI – 4.007	0.64	19	0.90
11.626 * NDVIre – 2.182	0.78	20	0.92
0.181 * RTVI$_{core}$ – 0.639	0.50	14	0.95
9.296 * –exp(–0.163* SR) + 6.910	0.60	20	0.90
20.17 * –exp(–0.692* SRre) + 7.329	0.39	19	0.96
Errors for soybean			
13.96 * gNDVI – 5.465	0.73	20	0.89
11.266 * NDVI – 4.007	0.65	18	0.76
11.626 * NDVIre – 2.182	0.90	30	0.88
0.181 * RTVI$_{core}$ – 0.639	0.97	30	0.88
9.296 * –exp(–0.163* SR) + 6.910	0.40	18	0.96
20.17 * –exp(–0.692 * SRre) + 7.329	0.54	21	0.92

Errors in this table were calculated from the validation dataset.

Table 6
Difference statistics of measured and estimated leaf biomass using the pooled regression coefficients (for combined crops).

Transfer functions	MAE (g/m^2)	CV (%)	r^2	*p*
Leaf biomass estimated from VIs – corn and soybean combined				
0.063 * EXP(9.659 * NDVI)	82.73	27	0.90	0.7067
16.037 * RTVI$_{core}$ – 229.63	130.33	24	0.79	0.0021
16.671 * SR – 4.804	104.58	195	0.43	0.0075
Total biomass estimated from VIs – corn and soybean combined				
0.502 * exp(11.091 * NDVIre)	249.53	62	0.62	0.000

P-value <0.05 indicates that the coefficients of the pooled crop regression model are significantly different from the coefficients of the individual crop regression model (at the 0.05 level). Transfer functions were calibrated on 70% of the 30 sampling site observations; and validated on 30% of the sampling site observations. Errors in this table were calculated from the validation dataset.

Table 7
Difference statistics of measured and estimated total biomass using crop specific regression models.

Transfer functions	MAE (g/m^2)	CV (%)	r^2
Total biomass estimated from integrated VIs – soybean			
92.408 * exp(0.037 * igNDVI)	157.94	62	0.67
17.26 * iMTVI2 – 82.339	84.63	38	0.95
208.95 * exp(0.026 * iNDVIre)	245.15	86	0.36
89.487 * exp(0.038 * iNDVI)	140.19	58	0.71
54.459 * exp(0.001 * iRTVI$_{core}$)	97.30	56	0.73
131.53 * exp(0.007 * iSRre)	184.92	70	0.58
0.772 * iSR – 2.849	77.84	45	0.87
Total biomass estimated from integrated VIs – corn			
49.085 * igNDVI – 681.66	796.09	114	0.96
45.292 * iMTVI2 – 247.49	267.22	37	0.73
50.711 * iNDVIre – 283.58	199.54	29	0.78
45.409 * iNDVI – 496.73	123.40	16	0.95
1.094 * iRTVI$_{core}$ – 12.522	155.72	23	0.95
8.247 * iSRre – 360.98	101.20	14	0.97
1.777 * iSR + 6.083	134.85	21	0.94

Transfer functions were calibrated on 70% of the 48 sampling site observations (24 corn, 24 soybean); and validated on 30% of the sampling site observations. Errors in this table were calculated from the validation dataset.

VIs for estimation of both leaf and total biomass with CV values ranging between 24 and 195% (Table 6). The NDVI performed best for estimation of leaf biomass and was also insensitive to crop type (Table 6). Independent validation of total biomass estimated from cumulative VIs demonstrated superior performance of iNDVI, iRTVI$_{core}$, iSR and iSRre for estimation of corn biomass, with CV values of 16, 23, 21 and 14%, respectively (Table 7). R^2 values ranged between 0.94 and 0.97. Errors were larger for estimation of soybean biomass, CV values ranged between 40 and 72%: iMTVI2 had the lowest CV. NDVI was used to create leaf biomass maps and iSRre was used to create total corn biomass maps for 2012 and 2013,

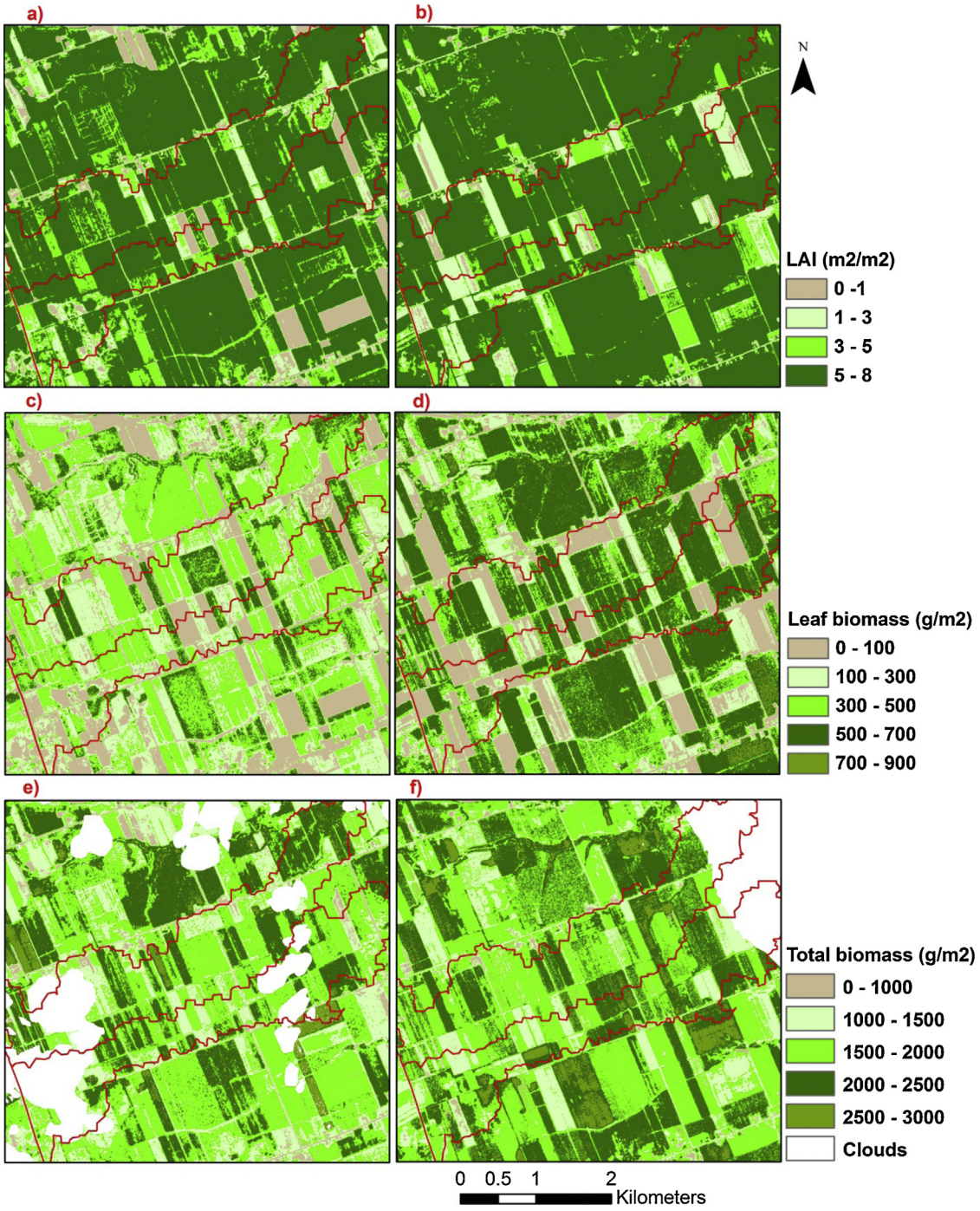

Fig. 9. Estimated peak growing season Biomass (a, b) for 2012 (a) and 2013 (b). And estimated peak growing season LAI (c, d) for 2012 (c) and 2013 (d). Peak growing season was between mid-July to mid-August. The 2012 image was from July 29, the 2013 image was from July 26. 2012 and 2013 were extreme dry and wet years, respectively. The total biomass map was calculated using all images from May to August.

as examples of contrasting exceptional dry (2012) and wet (2013) years (Fig. 9).

Continuous field crop LAI monitoring using RapidEye, Landsat and SPOT imagery

The use of multiple satellite sensors for near real-time crop monitoring increases the opportunity to obtain continuous information, bridging gaps in available imagery due to unexpected sensor failures or cloud cover. This concept exploits multiple satellite platforms as a virtual constellation. Multi-sensor approaches also permit exploitation of data from past years, accessing information from historical satellite archives. Such information can be used to analyze longer term trends in crop response to the effects of weather and land management practices, providing important information for future decision-making. RapidEye data are available from 2009. To support temporally continuous crop monitoring this analysis evaluated how LAI derived from Landsat and SPOT compares to LAI derived from RapidEye.

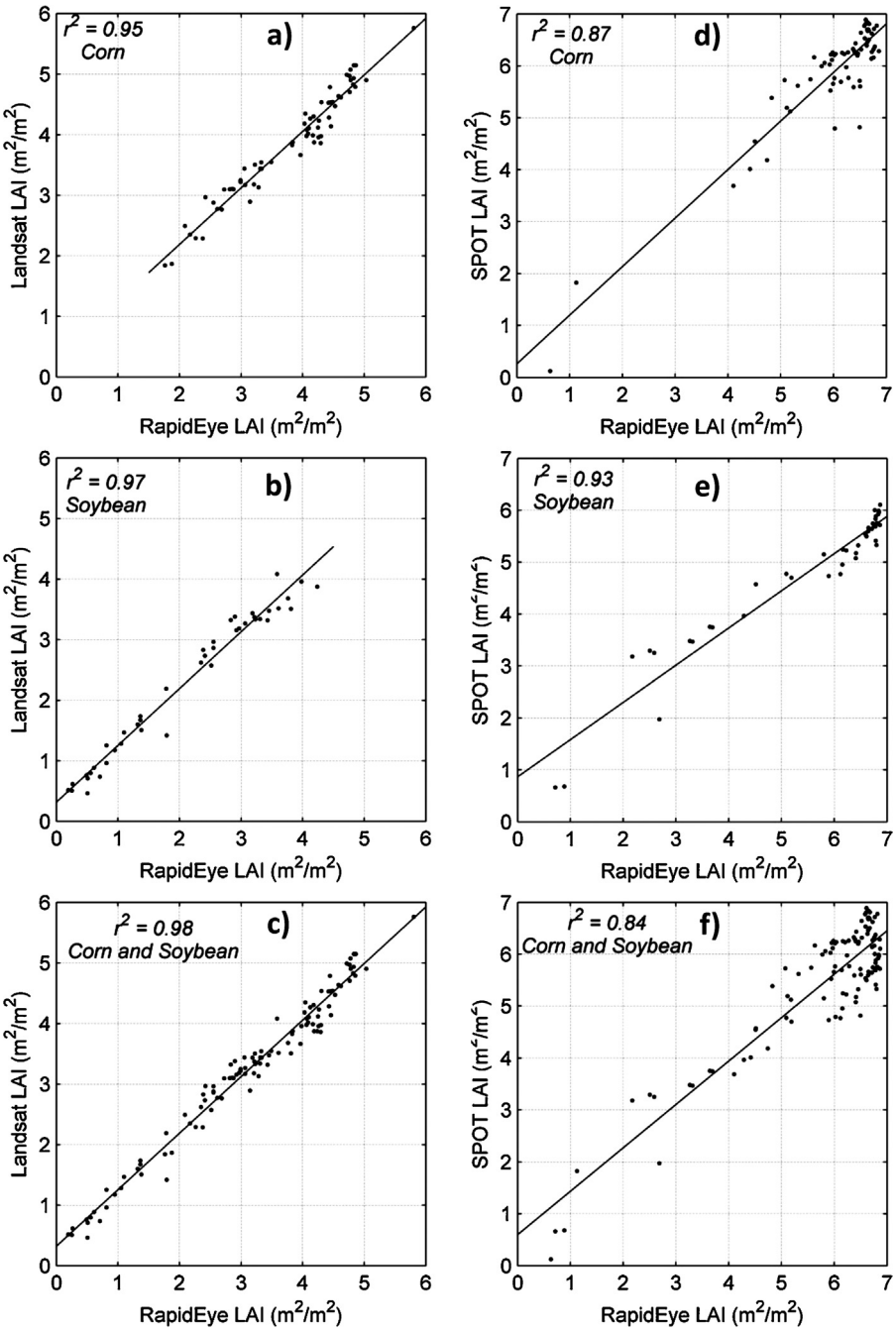

Fig. 10. Scatter plots of LAI estimated from Landsat, SPOT and RapidEye data: (a) corn LAI estimated from RapidEye and Landsat, (b) soybean LAI estimated from RapidEye and Landsat, (c) corn and Soybean LAI estimated from RapidEye and Landsat, (d) corn LAI estimated from RapidEye and SPOT, (e) soybean LAI estimated from RapidEye and SPOT and (f) corn and soybean LAI estimated from RapidEye and SPOT.

Best-fit functions were determined for matching Landsat, SPOT and RapidEye imagery and were compared to field-average LAI values between sensors. The results of this analysis should be interpreted with caution considering that the curve-fitting analysis was based on a few available site-observations. For both sensors, LSWI performed best for estimation of LAI (r^2 of 0.97 for Landsat, both crops, $n = 10$; r^2 of 0.98 for SPOT, both crops, $n = 13$). Landsat-derived field LAI correlated well with RapidEye-derived field LAI for individual and combined crops (r^2 ranging between 0.95 and 0.98, Fig. 10); with no significant differences between the average field LAI values (Fig. 11). Correlation analysis between the SPOT-derived field LAI and RapidEye-derived field LAI ranged between 0.84 and 0.93, but there was high scattering of the data points from the linear fit. The *t*-test showed a significant difference between RapidEye and SPOT LAI values of soybean fields.

These results indicate that an integration of data from multiple sensors could potentially support longer term monitoring of LAI based on sensor-dependant best-fit LAI transfer functions. This approach eliminates the need for spectral resampling of sensor reflectance, inter-calibration of VIs among sensors or spatial resampling of images from different sensors before estimating the LAI.

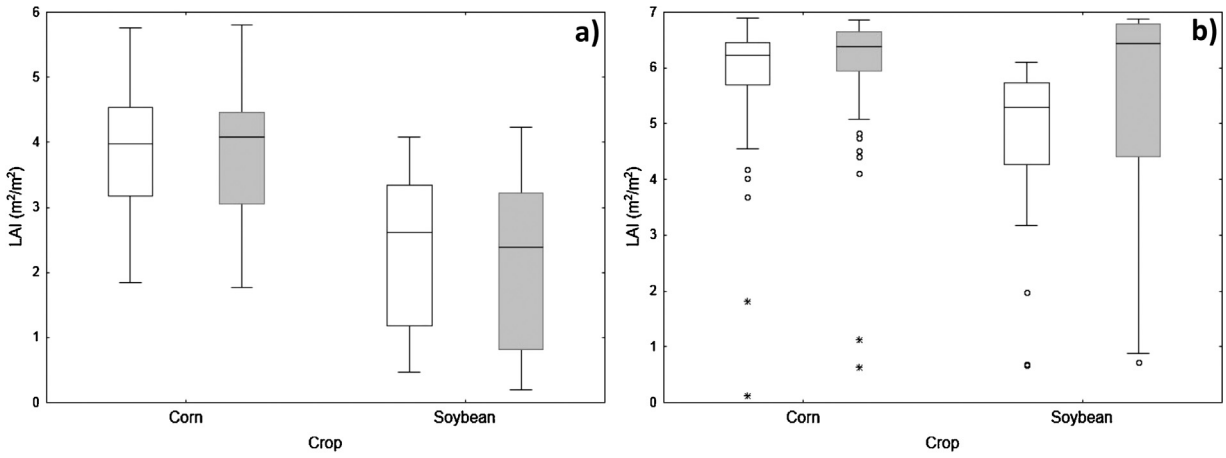

Fig. 11. Box plots of corn and soybean LAI estimated from (a) Landsat and RapidEye and (b) SPOT and RapidEye. In (a): White boxes represent Landsat LAI, gray boxes represent RapidEye LAI. In (b): White boxes represent SPOT LAI, gray boxes represent RapidEye LAI. In both panels: solid lines within the boxes represent the median. Box top and bottom represent the 75th and 25th percentile, respectively. Whisker ends represent the non-outlier minimum and maximum values. No significant differences between Landsat and RapidEye LAI for Corn ($p = 0.664$), for soybean ($p = 0.501$) or for Corn and Soybean combined ($p = 0.4976$). No significant differences between SPOT and RapidEye LAI for Corn ($p = 0.522$) or for Corn and Soybean combined ($p = 0.058$); but significant differences for soybean ($p = 0.042$).

Conclusions

Studies so far have not addressed the applicability of RapidEye's constellation for within-field corn and soybean LAI and biomass monitoring. This study demonstrated the utility of RapidEye data for obtaining crop information at relatively high spatial and temporal resolutions using VIs and transfer functions that are insensitive to crop type. Producers can use such crop information during the growing season for optimizing crop production.

Seven RapidEye VIs were evaluated for estimating LAI and biomass of corn and soybean, crops with contrasting leaf structures, canopy architectures and photosynthetic pathways. Overall, most of the indices had good linear or exponential relationships with LAI and showed sensitivity along the entire range of LAI values, from emergence to 8 m^2/m^2. The red-edge indices did not perform consistently better than the other indices, even though some indices showed more sensitivity to biomass than the non-red-edge indices. The green NDVI, NDVI and NDVIre were insensitive to crop-type; one LAI transfer function can be used for both crops without re-parameterization. Most indices saturated when leaf biomass was about 400 g/m^2, and when total biomass was around 800 g/m^2. Cumulative VIs performed well for estimation of total biomass, especially for corn. Finally, this study demonstrates the potential of using Landsat and SPOT images in a multi-sensor virtual constellation approach for continuous field LAI monitoring over time and space.

Acknowledgments

RapidEye imagery was provided under the Joint Experiment of Crop Assessment and Monitoring (JECAM) project. Financial support was provided by Agriculture and Agri-Food Canada's (AAFC) Integrated Water Resource and Management Project – South Nation Watershed and a visiting fellowship at AAFC from Natural Sciences and Engineering Research Council (NSERC) to A. Kross. The authors are thankful for the training on leaf area index data collection and processing provided by R. Fernandes (CCRS), J. Liu (AAFC) and J. Shang (AAFC). Many thanks to S. Homayouni, A. Liang, J. Nguyen, T. Chang, A. He and A. Pacheco for significant participation in the collection of field data. Thanks to G. Wilkes for providing us with land cover data and many thanks to R. McGregor for leading the 2011 field data collection campaign.

References

Bala, S.K., Islam, A.S., 2009. Correlation between potato yield and MODIS-derived vegetation indices. Int. J. Remote Sens. 30, 2491–2507.
Bastiaanssen, W.G.M., Molden, D.J., Makin, I.W., 2000. Remote sensing for irrigated agriculture: examples from research and possible applications. Agric. Water Manage. 46, 137–155.
Beckschäfer, P., Fehrmann, L., Harrison, R.D., Xu, J., Kleinn, C., 2014. Mapping leaf area index in subtropical upland ecosystems using rapideye imagery and the randomforest algorithm. iForest 7, 1–11.
Bolton, D.K., Friedl, M.A., 2013. Forecasting crop yield using remotely sensed vegetation indices and crop phenology metrics. Agric. For. Meteorol. 173, 74–84.
Brisson, N., Gary, C., Justes, E., Roche, R., Mary, B., Ripoche, D., Zimmer, D., Sierra, J., Bertuzzi, P., Burger, P., Bussière, F., Cabidoche, Y.M., Cellier, P., Debaeke, P., Gaudillère, J.P., Hénault, C., Maraux, F., Seguin, B., Sinoquet, H., 2003. An overview of the crop model STICS. Eur. J. Agron. 18, 309–332.
Broge, N.H., Leblanc, E., 2001. Comparing prediction power and stability of broadband and hyperspectral vegetation indices for estimation of green leaf area index and canopy chlorophyll density. Remote Sens. Environ. 76, 156–172.
Canisius, F., Fernandes, R., Chen, J., 2010. Comparison and evaluation of Medium Resolution Imaging Spectrometer leaf area index products across a range of land use. Remote Sens. Environ. 114, 950–960.
Chen, P., Tremblay, N., Wang, J., Vigneaulta, P., 2010. New index for crop canopy fresh biomass estimation. Spectrosc. Spectr. Anal. 30, 512–517 (in Chinese).
Chow, G.C., 1960. Tests of equality between sets of coefficients in two linear regressions. Econometrica 28, 591–605.
Cicek, H., Sunohara, M., Wilkes, G., McNairn, H., Pick, F., Topp, E., Lapen, D.R., 2010. Using vegetation indices from satellite remote sensing to assess corn and soybean response to controlled tile drainage. Agric. Water Manage. 98, 261–270.
Crabbé, P., Lapen, D.R., Clark, H., Sunohara, M., Liu, Y., 2012. Economic benefits of controlled tile drainage: Watershed Evaluation of Beneficial Management Practices, South Nation River basin, Ontario. Water Qual. Res. J. Canada 47, 30.
EC, 2014. Environment Canada, Russel Station, ON. http://weather.gc.ca (accessed 04.04.14).
Fang, H., Liang, S., Hoogenboom, G., 2011. Integration of MODIS LAI and vegetation index products with the CSM–CERES–Maize model for corn yield estimation. Int. J. Remote Sens. 32, 1039–1065.
Gao, B.-C., 1996. NDWI – a normalized difference water index for remote sensing of vegetation liquid water from space. Remote Sens. Environ. 58, 257–266.
Gitelson, A., Merzlyak, M.N., 1994. Spectral reflectance changes associated with autumn senescence of *Aesculus hippocastanum* L. and *Acer platanoides* L. Leaves. Spectral features and relation to chlorophyll estimation. J. Plant Physiol. 143, 286–292.
Gitelson, A.A., Kaufman, Y.J., Merzlyak, M.N., 1996. Use of a green channel in remote sensing of global vegetation from EOS-MODIS. Remote Sens. Environ. 58, 289–298.
Groten, S.M.E., 1993. NDVI – crop monitoring and early yield assessment of Burkina Faso. Int. J. Remote Sens. 14, 1495–1515.
Haboudane, D., Miller, J.R., Pattey, E., Zarco-Tejada, P.J., Strachan, I.B., 2004. Hyperspectral vegetation indices and novel algorithms for predicting green LAI of crop canopies: modeling and validation in the context of precision agriculture. Remote Sens. Environ. 90, 337–352.
Hunsaker, D.J., Barnes, E.M., Clarke, T.R., Fitzgerald, G.J., Pinter, P.J., 2005. Cotton Irrigation Scheduling Using Remotely Sensed and FAO-56 Basal Crop Coefficients. PN ETATS-UNIS: American Society of Agricultural Engineers, St. Joseph, MI.

Jiali, S., McNairn, H., Fernandes, R., Schulthess, U., Storie, J., 2012. Estimation of crop ground cover and leaf area index (LAI) of wheat using RapidEye satellite data: prelimary study. In: 2012 First International Conference on Agro-Geoinformatics (Agro-Geoinformatics), pp. 1–5.

Jordan, C.F., 1969. Derivation of leaf-area index from quality of light on the forest floor. Ecology 50, 663–666.

Liu, J., Pattey, E., Shang, J., Admira, S., Jégo, G., McNairn, H., Smith, A., Hu, B., Zhang, F., Freementle, J., 2009. Quantifying crop biomass accumulation using multi-temporal optical remote sensing observations. In: Proceedings of the 30th Canadian Symposium on Remote Sensing, pp. 22–25.

Liu, J., Pattey, E., Miller, J.R., McNairn, H., Smith, A., Hu, B., 2010. Estimating crop stresses, aboveground dry biomass and yield of corn using multi-temporal optical data combined with a radiation use efficiency model. Remote Sens. Environ. 114, 1167–1177.

Liu, J., Pattey, E., Jégo, G., 2012. Assessment of vegetation indices for regional crop green LAI estimation from Landsat images over multiple growing seasons. Remote Sens. Environ. 123, 347–358.

Luedeling, E., Hale, A., Zhang, M., Bentley, W.J., Dharmasri, L.C., 2009. Remote sensing of spider mite damage in California peach orchards. Int. J. Appl. Earth Obs. Geoinf. 11, 244–255.

Mahlein, A.-K., Oerke, E.-C., Steiner, U., Dehne, H.-W., 2012. Recent advances in sensing plant diseases for precision crop protection. Eur. J. Plant Pathol. 133, 197–209.

Mkhabela, M.S., Bullock, P., Raj, S., Wang, S., Yang, Y., 2011. Crop yield forecasting on the Canadian Prairies using MODIS NDVI data. Agric. For. Meteorol. 151, 385–393.

Monteith, J.L., 1972. Solar radiation and productivity in tropical ecosystems. J. Appl. Ecol. 9, 747–766.

Nguy-Robertson, A., Gitelson, A., Peng, Y., Viña, A., Arkebauer, T., Rundquist, D., 2012. Green leaf area index estimation in maize and soybean: combining vegetation indices to achieve maximal sensitivity. Agron. J. 104, 1336–1347.

National Topographic Data Base (NTDB), 2007. Government of Canada, Natural Resources Canada, Earth Sciences Sector, Centre for Topographic Information (Sherbrooke), www.geogratis.ca; ftp://ftp2.cits.rncan.gc.ca/pub/bndt/

Ontario Ministry of Food and Rural Affairs (OMAFRA), 2013. Corn: tillage. In: Agronomy Guide for Field Crops. OMAFRA Publ. 811. OMAFRA, Guelph, ON, Canada, http://www.omafra.gov.on.ca/english/crops/pub811/1tillage.htm (accessed 21.08.13).

OMAFRA, 2014. http://www.omafra.gov.on.ca/english/stats/crops (accessed 01.04.14).

Ramoelo, A., Cho, M., Mathieu, R., Skidmore, A., Schlerf, M., Heitkönig, I., 2012a. Estimating grass nutrients and biomass as an indicator of rangeland (forage) quality and quantity using remote sensing in savanna ecosystems. In: 9th International Conference of the African Association of Remote Sensing and the Environment (AARSE), El Jadida, Morroco, 28 October–2 November.

Ramoelo, A., Skidmore, A.K., Cho, M.A., Schlerf, M., Mathieu, R., Heitkönig, I.M.A., 2012b. Regional estimation of savanna grass nitrogen using the red-edge band of the spaceborne RapidEye sensor. Int. J. Appl. Earth Obs. Geoinf. 19, 151–162.

Rock, B.N., Vogelmann, J.E., 1985. Field and airborne spectral characterization of suspected acid deposition damage in red spruce (*Picea rubens*) from Vermont. In: Machine Processing of Remotely Sensed Data. Purdue Research Foundation, pp. 71.

Rouse, J.W., Haas, R.H., Schell, J.A., 1974. Monitoring the Vernal Advancement and Retrogradation (Greenwave Effect) of Natural Vegetation. Texas A and M University, College Station.

Scharf, P.C., Lory, J.A., 2002. Calibrating corn color from aerial photographs to predict sidedress nitrogen need contrib. from the Missouri Agric. Exp. Stn. J. Ser. No. 13086. Agron. J. 94, 397–404.

Steduto, P., Hsiao, T.C., Raes, D., Fereres, E., 2009. AquaCrop – the FAO Crop Model to Simulate Yield Response to Water: I. Concepts and Underlying Principles All rights reserved no part of this periodical may be reproduced or transmitted in any form or by any means, electronic or mechanical, including photocopying, recording, or any information storage and retrieval system, without permission in writing from the publisher. Agron. J. 101, 426–437.

Strachan, I.B., Stewart, D.W., Pattey, E., 2005. Determination of leaf area index in agricultural systems. In: Hatfield, J.L., Baker, J.M. (Eds.), Micrometeorology in Agricultural Systems. American Society of Agronomy, Inc., Crop Science Society of America, Inc., Soil Science Society of America, Inc., Madison, WI, USA, pp. 179–198, Agronomy Monograph No. 47 ASA-CSSA-SSSA.

Sunohara, M., Craiovan, E., Topp, E., Gottschall, N., Drury, C., Lapen, D., 2014a. Comprehensive nitrogen budgets for controlled tile drainage fields in Eastern Ontario, Canada. J. Environ. Qual. 43, 617–630.

Sunohara, M.D., Gottschall, N., Wilkes, G., Craiovan, E., Topp, E., Que, Z., Seidou, O., Frey, S., Lapen, D.R., 2014b. Long term observations of nitrogen and phosphorus export in paired-agricultural watersheds under controlled and conventional tile drainage management. J. Environ. Qual. (in review).

Viña, A., Gitelson, A.A., Nguy-Robertson, A.L., Peng, Y., 2011. Comparison of different vegetation indices for the remote assessment of green leaf area index of crops. Remote Sens. Environ. 115, 3468–3478.

Vuolo, F., Atzberger, C., Richter, K., D'Urso, G., Dash, J., 2010. Retrieval of biophysical vegetation products from RapidEye imagery. ISPRS TC VII Symposium – 100 Years ISPRS, vol. 38. ISPRS, Vienna, Austria, pp. 281–286.

Willmott, C.J., 1982. Some comments on the evaluation of model performance. Bull. Am. Meteorol. Soc. 63, 1309–1313.

Zhang, N., Wang, M., Wang, N., 2002. Precision agriculture – a worldwide overview. Comput. Electron. Agric. 36, 113–132.

Zhang, X., Friedl, M.A., Schaaf, C.B., Strahler, A.H., Hodges, J.C.F., Gao, F., Reed, B.C., Huete, A., 2003. Monitoring vegetation phenology using MODIS. Remote Sens. Environ. 84, 471–475.